
Uni6Dv2: Noise Elimination for 6D Pose Estimation

Mingshan Sun
SenseTime Research
sunmingshan@sensetime.com

Ye Zheng
Institute of Computing Technology
Chinese Academy of Sciences
zhengye@ict.ac.cn

Tianpeng Bao
SenseTime Research
baotianpeng@sensetime.com

Jianqiu Chen
Harbin Institute of Technology, Shenzhen
jianquier@gmail.com

Guoqiang Jin
SenseTime Research
jinguoqiang@sensetime.com

Rui Zhao
SenseTime Research
zhaorui@sensetime.com

Liwei Wu
SenseTime Research
wuliwei@sensetime.com

Xiaoke Jiang
SenseTime Research
jiangxiaoke@sensetime.com

Abstract

Few prior 6D pose estimation methods use a backbone network to extract features from RGB and depth images, and Uni6D is the pioneer to do so. We find that primary causes of the performance limitation in Uni6D are Instance-Outside and Instance-Inside noise. Uni6D inevitably introduces Instance-Outside noise from background pixels in the receptive field due to its inherently straightforward pipeline design, and ignores the Instance-Inside noise in the input depth data. In this work, we propose a two-step denoising method to handle aforementioned noise in Uni6D. In the first step, an instance segmentation network is used to crop and mask the instance to remove noise from non-instance regions. In the second step, a lightweight depth denoising module is proposed to calibrate the depth feature before feeding it into the pose regression network. Extensive experiments show that our method called Uni6Dv2 is able to eliminate the noise effectively and robustly, outperforming Uni6D without sacrificing too much inference efficiency. It also reduces the need for annotated real data that requires costly labeling.

1 Introduction

6D pose estimation is essential for emerging applications such as intelligent robotic grasping [1, 2], autonomous driving [3–5], and augmented reality [6]. The primary goal of 6D pose estimation is to determine the 6D pose of an object, which includes its location and orientation. The RGB-D sensor can augment the conventional RGB image with depth information in a per-pixel basis and provide directly geometry information, making it a more appealing data source for 6D pose estimation as it becomes more feasible and affordable. The only fly in the ointment is that it inevitably introduces physical noise when acquiring depth information [7–11].

Considering the heterogeneity of RGB data and depth data, previous state-of-the-art methods [12–14] typically handle them with two backbone networks separately, in which, 2D CNN is used for RGB data and PointNet [15] or PointNet++ [16] for depth data. Recently, a new approach called Uni6D [17]

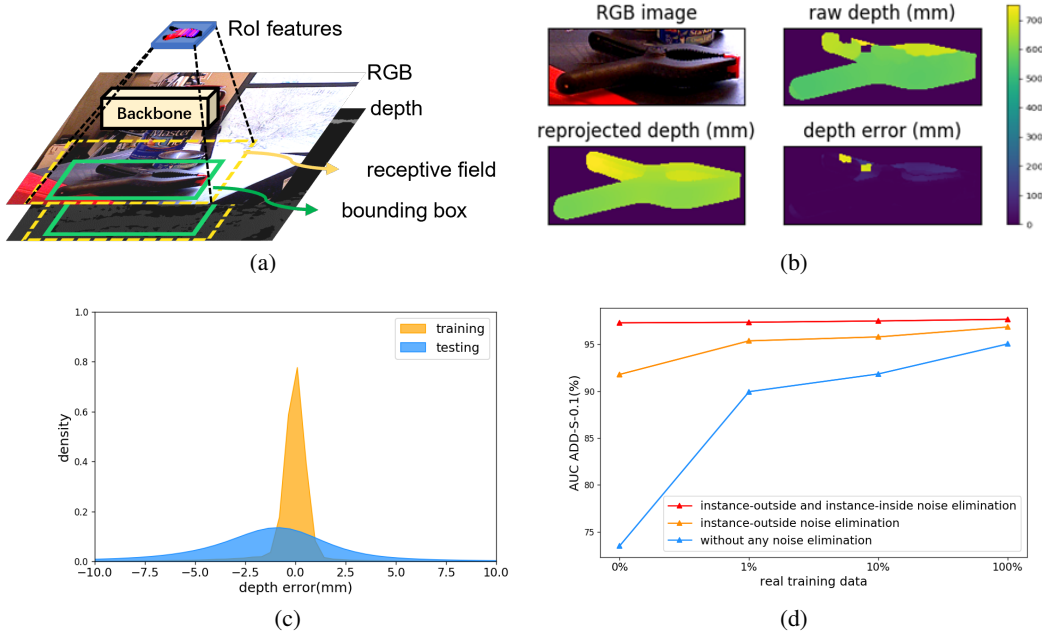


Figure 1: Illustration of noise problem in 6D pose estimation. (a) Examples of instance-outside noise. (b) Examples of instance-inside noise. (c) Quantitative results of instance-inside noise according to the depth reprojection error statistics. (d) Uni6D results under various real data percentages and noise elimination methods. Eliminating the noise improves performance while lowering the need for real data in training set.

subverts the above practice by adding extra UV information, i.e., coordinates of each pixel, into the RGB-D input to solve the "projection breakdown" [17] issue. It leverages basic framework of Mask R-CNN[18], including RPN, RoI Align, and especially the unified CNN backbone to extract features from RGB and depth images possible, resulting in an efficient and straightforward realization pipeline. However, Uni6D ignores the potential pitfalls hidden in its straightforward pipeline and the input depth data, severely limiting its performance.

We find that the main sources of Uni6D’s potential pitfalls are two types of noise: instance-outside noise introduced by the RoI-based 6D pose estimation methodology, and instance-inside noise from the unreliable depth data. As shown in Fig. 1(a), the instance-outside noise comes from the background pixels outside the target instances, and Uni6D introduced it in the pose regression with its detection and pose regression pipeline. Since the deep features of CNN have corresponding receptive fields, the information out of the instance will also be included in the RoI features obtained by the RPN and RoI Align. Because the feature outside the instance isn’t useful for pose estimation, this background information can even interference the pose regression. For the instance-inside noise, it is introduced by depth sensor during capturing depth information, as exemplified in Fig. 1(b).

To quantify the above noise and their impact, we construct several corresponding experiments. As shown in Fig. 1(c), we provide the statistic of instance-inside noise of the YCB-Video [19] dataset by calculating the depth deviation according to depth reprojection error, which indicates that there is depth noise in the dataset. Then, we investigate the effects of performance by removing these kinds of noise incrementally in Fig. 1(d). We use the ground truth bounding box and mask to crop and mask the RoI of each instance to filter out instance-outside noise. We use the depth calculated by reprojection as the ground truth to remove instance-inside noise. We can observe that removing these two types of noise gradually can significantly improve the accuracy on the YCB-Video dataset, and reduce the need for real data to train the model. According to above experimental results, we believe that each kind of noise will affect the performance of the model. Worse still, limited by the high cost of annotation, existing datasets such as YCB-Video [19] and LineMOD [20] include a lot of synthetic data without depth noise in training set and put the real data with depth noise in test set. This train-test gap as shown in Fig. 1(c) further amplifies the negative effect of depth noise.

To this end, we propose Uni6Dv2, a two-step denoising 6D pose estimation method based on the simple yet effective design. The first step aims to address the instance-outside noise, and Uni6Dv2 predicts the instance segmentation mask of each instance from the RGB-D image to filter out irrelevant non-instance pixels. In the second step, a depth denoising module is used to correct the depth feature with corresponding depth normal and XY before feeding them into the subsequent pose regression network.

The main contributions of this work are: 1) we uncover different potential noise that severely limit the performance of RoI-based 6D pose estimation methods, and categorize them as instance-outside noise and instance-inside noise; 2) we propose a two-step denoising pipeline to address the noise problem in the original Uni6D, which uses the instance segmentation network to filter out the instance-outside noise in the first step and a depth denoising module to handle instance-inside noise in the second step; 3) our approach advances state-of-the-art by 0.2% on the AUC ADD-S metric and achieves 91.5% on the AUC ADD(S) metric for YCB-Video dataset. In particular, the performance outperforms Uni6D by a large margin, especially in scenes with insufficient real data.

2 Related Work

2.1 6D Pose Estimation

In accordance with calculation methods of 6D pose parameters, we divide 6D pose estimation methods into two types: keypoint-based and RoI-based methods.

Keypoint-based methods. The 6D pose parameters in keypoint-based methods are estimated by a PnP algorithm matching the predicted keypoints and target keypoints. The prediction of 2D keypoints in prior methods are usually from direct regression [21–23] or heatmaps [24–26]. Considering robustness in truncated and occluded scenes, PVNet [27] proposes a voting network to obtain the dense prediction of 2D keypoints of objects and utilizes an uncertainty-driven PnP algorithm to improve performance. Recent methods [13, 14] extend keypoint detection to 3D space by predicting each 3D point semantic label and offsets to pre-defined target keypoints. To calculate keypoints in the camera coordinates system and distinguish different objects, an iterative voting mechanism is adopted to vote for the best prediction of keypoints based on the offsets and semantic labels. The final 6D pose parameters are predicted by an iterative least-squares regression algorithm fitting predicted 3D keypoints with corresponding pre-defined 3D target keypoints. However, the iterative voting and regression operations in these methods are time-consuming and heavy in practical applications.

RoI-based methods. To estimate 6D pose of a single instance from the image with multiple instances, RoI-based methods crop each instance by the candidate RoI prediction and then feed each RoI region image patch or feature into the pose regression network to estimate the 6D pose directly. PoseCNN [19] utilizes two RoI pooling layers [28] to extract the corresponding visual feature to regress the quaternion representing rotations. Based on the RoI feature from RGB images, following methods [29–31] improve the computation method of rotation as well as translation and introduce extra class and geometric priors. However, the insufficiency of geometry information limits the performance of these methods. To make use of geometry information, DenseFusion [12] and ES6D [32] crop the RoI region from both RGB and depth images and then concatenate them as the input of pose regression network. In practice, the crop and RoI-pooling operations in these CNN pipelines lead to spatial transformation, which breaks the 2D-3D projection equation. Uni6D [17] is the first to expose the "projection breakdown" problem and solve it by adding extra UV information into the RGB-D input. Hence, it can adopt a single CNN backbone to process heterogeneous data sources. However, the performance of the method degrades when there is noise in the candidate RoI regions. In the following, we conduct an in-depth and systematic analysis of the denoising operation in 6D pose estimation, which can alleviate the interference from noise.

2.2 Denoising operation in 6D Pose Estimation

Through the investigation of the existing 6D pose estimation methods, the potential denoising operation mainly includes two types: vote-based denoising and mask-based denoising.

Vote-based denoising. The voting mechanism is adopted to iteratively vote the centroid or keypoints based on the dense pixel-level prediction. The inlier pixels that vote for keypoints are devoted to predicting the final pose estimation. The rest unvoted pixels viewed as inaccurate predictions are

not involved in the final decision, thus performing denoising in an implicit way. PoseCNN[19] estimates 2D object centroid by the vote of the pixel-wise prediction for the object center direction vector instead of directly regressing the coordinates. The voting mechanism filters the unvoted pixels' prediction alleviating the interference from noise. For keypoint prediction, PVNet [27] adopts the same vote mechanism to estimate the location of 2D keypoints by the pixel-wise vector-field prediction. To extend keypoints detection from 2D to 3D, PVN3D [13] and FFB6D [14] vote 3D keypoints and estimate the 6D pose by iteratively fitting prediction and target pre-defined keypoints. The fitting algorithm has ability to weaken the noise in the instance-inside points. However, the iterative voting and fitting as a denoising operation are inefficient and heavy, which account for most of the total frame processing time.

Mask-based denoising. Mask operation in the prior works aims to eliminate the noise from instance-outside regions in the feature-level. These features from the instance-outside regions interfere with the target instance feature representation and affect the 6D pose regression. To obtain the instance mask, many methods [19, 29, 30, 33, 32] adopt a two-stage scheme. In the first stage, a instance segmentation network is adopted to predict semantic segmentation masks and bounding boxes for each target instance. In the second stage, a pose estimation network is proposed to predict the 6D pose based on the cropped or masked instance-inside region. Therefore, the final 6D pose is mainly from the estimation of the instance-inside points, suppressing the interference of instance-outside noise. To further weakens the possible interference from the instance-outside noise, recent work ES6D[32] estimates 6D pose only based on the point with the highest confidence score. However, since the instance-outside region still exists in the input image, the coarse intermediate features masking would inevitably retain the information from the noise region within the receptive field. To comprehensively suppress noise, we systematically analyze the type as well as source of noise and propose a novel two-step pipeline with a lightweight depth denoising module to address the noise issue.

3 Approach

Our work can be viewed as an extension of Uni6D [17] with a novel two-step denoising pipeline. We first review Uni6D (Sec. 3.1), and then give the details of the proposed method includes the denoising processes of instance-outside noise and instance-inside noise (Sec. 3.2). Finally, the details of loss function are provided (Sec. 3.3).

3.1 Review of Uni6D: a Unified CNN Framework for 6D Pose Estimation

Uni6D fixed the "projection breakdown" issue caused by the CNN operation and spatial transformations by adding extra UV information (Plain UV, XY, PE) with NRM together to RGB-D images, allowing for simultaneous feature extraction of RGB and depth data with an unified network. It took the structure of Mask R-CNN and added extra RT head and abc head to directly estimate the 6D pose, achieving impressive results on existing 6D pose estimation benchmarks. However, it introduced instance-outside noise from background pixels and ignored instance-inside noise in the input depth data. We will introduce our two-step denoising method next to address these issues.

3.2 Comprehensive Denoising Pipeline

To effectively suppress the instance-outside and instance-inside noise, we propose a novel two-step denoising pipeline named Uni6Dv2, which is illustrated in Fig. 2. Our method is based on Uni6D's basic methodology, which involves adding various UV information to input RGB-D data and regressing 6D pose directly. The instance-outside noise is handled in the first denoising step. For an input RGB-D image, we perform instance segmentation with Mask R-CNN to filter out the instance-outside pixels in RGB, depth, Plain UV, XY, NRM and corresponding PE. The above data is then fed into the second step. A depth denoising module and a depth reconstruction task are proposed in the second denoising step to calibrate the feature extracted from the data output by the first step, making it easier for subsequent networks to regress more accurate 6D pose. We use Uni6D's RT head to regress the 6D pose directly, while keeping the same abc head as the auxiliary training branch.

Instance-outside Noise Elimination. The most intuitive and efficient choice to filter out the instance-outside noise is directly discarding non-instance regions on the feature map. However, this feature-level operation can not completely remove the background feature noise because deep features in

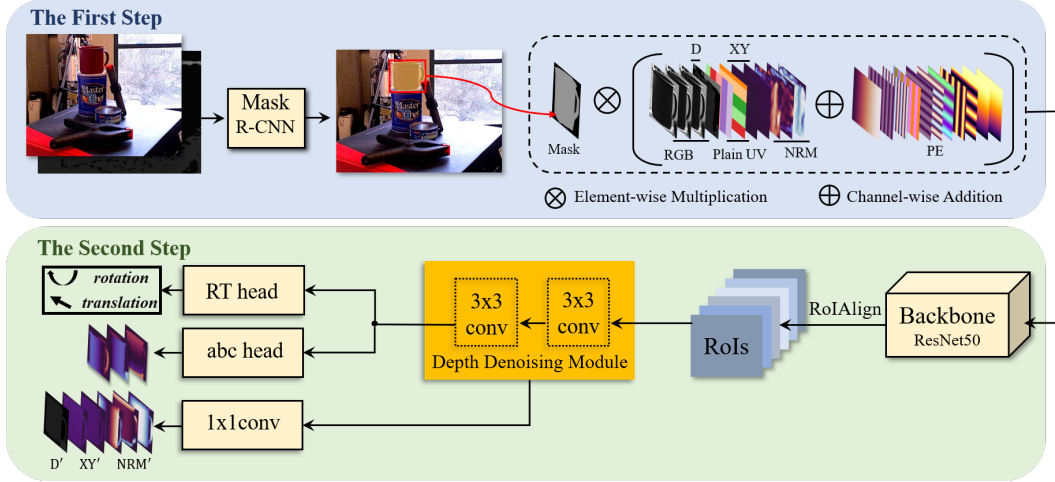


Figure 2: Overview architecture of Uni6Dv2, which includes two denoising steps. The first step removes instance-outside noise by adopting the Mask R-CNN to crop and mask the information about the instance. The second step focuses on the instance-inside noise, which uses a depth denoising module and a depth information estimation auxiliary task to calibrate depth feature before the 6D pose regression. The auxiliary supervision labels D' , XY' and NRM' are calculated base on reprojection.

CNN have a certain receptive field, and the features at the area of the target instance also contains a certain range of surrounding background information. As a result, rather than using the easiest-to- envisage feature-level method, we must filter out the instance-outside noise at the image level. We use Mask R-CNN to obtain the bounding boxes and segmentation results for all instances in the input RGB-D image. A majority of instance-outside noise is eliminated by cropping RGB-D patches according to the bounding box. And the rest of instance-outside noise, which remains in the bounding box, is further removed by masking cropped patches with segmentation results. Corresponding Plain UV, XY, and NRM and PE are also cropped and masked.

Instance-inside Noise Elimination. As shown in Fig. 1(b), the instance-inside noise contains holes and numerical errors in the depth image, both of which affect the performance of the 6D pose estimation task. A widely used method utilizes the classical processing algorithm [34] to fill holes in the raw depth image before regressing the 6D pose. However, the filled pixels in the depth image may still has numerical errors limited by the non-parametric pre-processing method. To handle the instance-inside noise more effectively, we propose a learnable parametric depth denoising module with a depth estimation task to calibrate the depth information contained in the features. As shown in the second step of Fig. 2, features extracted from RoI Align are fed into our depth denoising module before used to regress the 6D pose. To aid in the convergence of the depth denoising model, we add an auxiliary reconstruction task which regresses the noiseless depth, XY, and NRM simultaneously through a 1×1 convolutional layer. The supervision labels of the noiseless depth, XY, and NRM are obtained by reprojection from the CAD model. This lightweight depth denoising module can effectively calibrate depth information in features without reducing inference efficiency significantly.

3.3 Loss Function

The loss function of the entire network includes the respective loss functions of the two steps. The Mask R-CNN is first trained to converge with its original loss. Then, we freeze the parameters of the first step and train the network in the second step with the RT regression loss, abc regression loss, and the novel depth denoising loss. The RT regression loss \mathcal{L}_{rt} is defined as:

$$\mathcal{L}_{rt} = \frac{1}{m} \sum_{x \in \mathcal{O}} \|(Rx + T) - (R^*x + T^*)\|, \quad (1)$$

where \mathcal{O} denotes the vertex set of object's points from the 3D model, R and T are the rotation matrix and the translation vector, $*$ denotes the ground truth and m is the number of points in \mathcal{O} . The abc

regression loss is:

$$\mathcal{L}_{abc} = |a - a^*| + |b - b^*| + |c - c^*|, \quad (2)$$

where (a, b, c) are the coordinates of visible points. The depth denoising loss is:

$$L_{depth} = |d - d^*| + |x - x^*| + |y - y^*| + |n_x - n_x^*| + |n_y - n_y^*| + |n_z - n_z^*|, \quad (3)$$

where d is the depth and (n_x, n_y, n_z) are the coordinates of depth normal calculated from depth, (x, y) is the visible point’s coordinate in camera coordinate system. Finally, the overall loss function of the second step is:

$$\mathcal{L} = \lambda_0 \mathcal{L}_{rt} + \lambda_1 \mathcal{L}_{abc} + \lambda_2 \mathcal{L}_{depth}, \quad (4)$$

where λ_0, λ_1 and λ_2 are the weights for each loss.

4 Experiments

4.1 Benchmark Datasets

We compare the proposed method with others on three benchmark datasets.

YCB-Video [35] contains 92 RGB-D videos with 21 YCB objects, which has depth noise and occlusions. Following previous work [19, 13, 12, 17], we add synthetic images for training and the synthetic ratio is 83.17%. We also apply the hole completion algorithm used in [13, 17] to improve depth images.

LineMOD [20] contains 13 videos of 13 low-textured objects. Following previous work [36, 19, 13, 17], we also add synthetic images for training and the synthetic ratio is 99.71%.

Occlusion LineMOD [37] is selected from the LineMOD dataset, which has heavily occluded objects, making the scenes more challenging.

4.2 Evaluation Metrics

We use the average distance metrics ADD and ADD-S to evaluate our method, following [19, 12, 14, 17]. The ADD metric [38] is calculated as follow:

$$ADD = \frac{1}{m} \sum_{x \in \mathcal{O}} \|(Rx + T) - (R^*x + T^*)\|, \quad (5)$$

where m is the total vertex number, x indicates any vertex of the 3D model \mathcal{O} , $[R, T]$ and $[R^*, T^*]$ are predicted pose and ground truth pose respectively. The ADD-S is similar to ADD, but is used to measure the performance of symmetric objects, which is based on the closest point distance:

$$ADD-S = \frac{1}{m} \sum_{x_1 \in \mathcal{O}} \min_{x_2 \in \mathcal{O}} \|(Rx_1 + T) - (R^*x_2 + T^*)\|. \quad (6)$$

For YCB-Video dataset, the area under the accuracy-threshold curve obtained by varying the distance threshold with a maximum threshold of 0.1 meters (AUC ADD-S and ADD(S)) is reported, following [19, 12–14]. The ADD(S) means measure asymmetric object by ADD and symmetric object by ADD-S. For LineMOD and Occlusion LineMOD datasets, the accuracy of distance less than 10% of the objects’ diameter (ACC ADD-0.1d) is reported, following [36, 14]

4.3 Comparison with Other Methods

We compare our method with others on YCB-Video, LineMOD, and Occlusion LineMOD datasets. The results of YCB-Video dataset are presented in main paper and the results of LineMOD and Occlusion LineMOD are shown in our Appendix.

Table 1: Evaluation results on the YCB-Video dataset. Symmetric objects are denoted in bold.

Object	PoseCNN [19]		DenseFusion [12]		PVN3D [13]		FFB6D [14]		Uni6D [17]		Ours	
	ADD-S	ADD(S)	ADD-S	ADD(S)	ADD-S	ADD(S)	ADD-S	ADD(S)	ADD-S	ADD(S)	ADD-S	ADD(S)
002_master_chef_can	83.9	50.2	95.3	70.7	96	80.5	96.3	80.6	95.4	70.2	96.0	74.2
003_cracker_box	76.9	53.1	92.5	86.9	96.1	94.8	96.3	94.6	91.8	85.2	96.0	94.2
004_sugar_box	84.2	68.4	95.1	90.8	97.4	96.3	97.6	96.6	96.4	94.5	97.6	96.6
005_tomato_soup_can	81.0	66.2	93.8	8.47	96.2	88.5	95.6	89.6	95.8	85.4	96.1	86.6
006_mustard_bottle	90.4	81.0	95.8	90.9	97.5	96.2	97.8	97.0	95.4	91.7	97.8	96.7
007_tuna_fish_can	88.0	70.7	95.7	79.6	96.0	89.3	96.8	88.9	95.2	79.0	96.3	76.0
008_pudding_box	79.1	62.7	94.3	89.3	97.1	95.7	97.1	94.6	94.1	89.8	96.6	94.7
009_gelatin_box	87.2	75.2	97.2	95.8	97.7	96.1	98.1	96.9	97.4	96.2	98.0	97.0
010_potted_meat_can	78.5	59.5	89.3	79.6	93.3	88.6	94.7	88.1	93.0	89.6	95.7	91.9
011_banana	86.0	72.3	90.0	76.7	96.6	93.7	97.2	94.9	96.4	93.0	98.0	96.9
019_pitcher_base	77.0	53.3	93.6	87.1	97.4	96.5	97.6	96.9	96.2	94.2	97.5	96.9
021_bleach_cleanser	71.6	50.3	94.4	87.5	96.0	93.2	96.8	94.8	95.2	91.1	97.0	95.3
024_bowl	69.6	69.6	86.0	86.0	90.2	90.2	96.3	96.3	95.5	95.5	96.8	96.8
025_mug	78.2	58.5	95.3	83.8	97.6	95.4	97.3	94.2	96.6	93.0	97.7	96.3
035_power_drill	72.7	55.3	92.1	83.7	96.7	95.1	97.2	95.9	94.7	91.1	97.6	96.8
036_wood_block	64.3	64.3	89.5	89.5	90.4	90.4	92.6	92.6	94.3	94.3	96.1	96.1
037_scissors	56.9	35.8	90.1	77.4	96.7	92.7	97.7	95.7	87.6	79.6	95.0	90.3
040_large_marker	71.7	58.3	95.1	89.1	96.7	91.8	96.6	89.1	96.7	92.8	97.0	93.1
051_large_clamp	50.2	50.2	71.5	71.5	93.6	93.6	96.8	96.8	95.9	95.9	97.0	97.0
052_extra_large_clamp	44.1	44.1	70.2	70.2	88.4	88.4	96.0	96.0	95.8	95.8	96.5	96.5
061_foam_brick	88.0	88.0	92.2	92.2	96.8	96.8	97.3	97.3	96.1	96.1	97.4	97.4
Avg	75.8	59.9	91.2	82.9	95.5	91.8	96.6	92.7	95.2	88.8	96.8	91.5

4.3.1 Evaluation on YCB-Video Dataset

We present the quantitative results of the proposed Uni6Dv2 on YCB-Video dataset in Table 1. Compared with other methods, our approach advances state-of-the-art results by 0.2% on the ADD-S metric and achieves 91.5% on the ADD(S) metric. It is worth emphasizing that Uni6Dv2 comprehensively exceeds Uni6D, especially on objects with fewer pixels. For example, "037_scissors" of Uni6Dv2 achieves 7.36% improvement on the ADD-S metric and 9.72% on the ADD(S).

4.3.2 Time Efficiency

We compare the inference speed of our method with PoseCNN [19], DenseFusion [12], PVN3D [13], FFB6D [14], and Uni6D [17] in Table 2 and Fig. 3, our method still maintains time efficiency than the method with two heterogeneous backbones, which is $6\times$ faster than FFB6D, and $11\times$ than PVN3D. More specifically, the first and second steps of our method take 35 ms and 12 ms, the extra computation is mainly added on the backbone in the second step, so it is a little slower than Uni6D.

Table 2: Time cost and frames per second (FPS) on YCB-Video Dataset. The results of PoseCNN and DenseFusion come from [12], which does not specify the type of device used.

Method	Network/ms	Post-process/ms	All/ms	FPS
PoseCNN [19]	200	0	200	5
DenseFusion [12]	50	10	60	16.67
PVN3D [13]	110	420	530	1.89
FFB6D [14]	20	260	280	3.57
Uni6D [17]	39	0	39	25.64
Ours	47	0	47	21.27

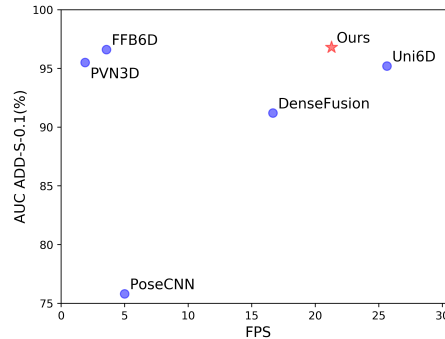


Figure 3: Comparison of accuracy and inference speed on the YCB-Video dataset.

4.4 Ablation Study

4.4.1 Effect of Noise Elimination

To investigate the contribution of the proposed noise elimination operations in our method, we superimpose these denoising operations gradually. In this comparison, we divide instance-outside

Table 3: Comparison of different types of denoising on the YCB-Video dataset.

Denoising level			Based on GT		Based on DT	
Box	Mask	Depth	ADD(S)	ADD-S	ADD(S)	ADD-S
			-	-	95.18	88.83
✓			96.39	90.58	96.01	89.80
✓	✓		96.85	91.55	96.52	91.27
✓	✓	✓	97.67	92.52	96.77	91.51

Table 5: Comparison of mask quality for instance-outside denoise on the YCB-Video dataset.

Input of Mask-RCNN	mIoU	ADD-S	ADD(S)
RGB-D with UV	78.15	96.52	91.28
RGB-D	80.43	96.77	91.51
RGB	80.21	96.79	91.41

Table 4: Comparison of mask strategies for instance-outside denoise on the YCB-Video dataset.

Denoising strategy	ADD-S	ADD(S)
no denoising	95.18	88.83
feature-level	96.25	90.21
image-level	96.52	91.27

Table 6: Comparison of instance-inside denoise strategies on the YCB-Video dataset.

Depth	XY	NRM	ADD-S	ADD(S)
			96.52	91.27
✓			96.51	90.30
✓	✓		96.74	91.26
✓		✓	96.74	91.23
✓	✓	✓	96.77	91.51

noise into the noise in box and the noise out of box, and eliminate them by cropping and masking. Uni6D without any denoising operation is our baseline. In Table 3, "Box" denotes cropping the input data by detection bounding boxes to eliminate the noise in the background out of the box. "Mask" means filtering out the background noise in the box, and "Depth" denotes calibrating the depth feature through the depth denoising module. The "Box" and "Mask" is used together for instance-outside noise elimination and "Depth" is for instance-inside noise elimination. "Based on GT" means using the ground truth of detection, segmentation and reprojection depth to train the pose regression model, it indicates that eliminating every noise increases the upper bound on performance. "Based on DT" is the experimental result of our method without any ground truth leaking. Using the first denoise step to remove instance-outside noise brings 1.34% improvement in ADD-S and 1.44% in ADD(S). And the second denoise step brings 0.25% improvement in ADD-S and 0.24% in ADD(S).

4.4.2 Comparison of Denoising Strategies

To further explore the effect of our two-step denoising method, we compare different denoising strategies of instance-outside noise and instance-inside noise.

For instance-outside noise, there are two optional strategies includes feature-level and image-level. The feature-level strategy crops and masks the feature map directly, which can reduce computational complexity. However, the information from the background around the instance introduced by the receptive field is still present in the cropped and masked feature, limiting the denoising effect. Therefore, we adopt the image-level strategy in first step and results in Table 4 prove that it brings 0.27% improvement in ADD-S and 1.06% in ADD(S) compared with the feature-level strategy. Another advantage of using image-level denoising strategy for instance-outside noise is that it allows us to avoid introducing UV information in the input of instance segmentation network. The UV information can break the convolution translation invariance and affects the quality of detection and segmentation. To verify the effect of different inputs for Mask-RCNN, we employ RGB, RGB-D and RGB-D with UV into Mask-RCNN. As shown in Table 5, introducing UV in Mask R-CNN decreases the performance and using RGB-D image as the input data is better.

For instance-inside noise, we explore the effect of adding different depth-related information as the supervised label, including the re-projected depth, XY and NRM. Results in Table 6 show that using all depth-related information strengthen the effect of denoising, which brings 0.25% improvement in ADD-S and 0.28% in ADD(S).

4.4.3 The Superiority of Reducing Real Data Requirements

We randomly sample 0%, 1% and 10% of the real training data and fused them with synthetic data as new training datasets, verify the superiority of our denoising method on reducing real data requirements. The test dataset keeps the original setting. The experiment results of Uni6D, denoise with ground truth and our method are shown in Table 7. With the proportion of real data decreases, our method can still maintain high performance, which benefits from its two-step denoising pipeline.

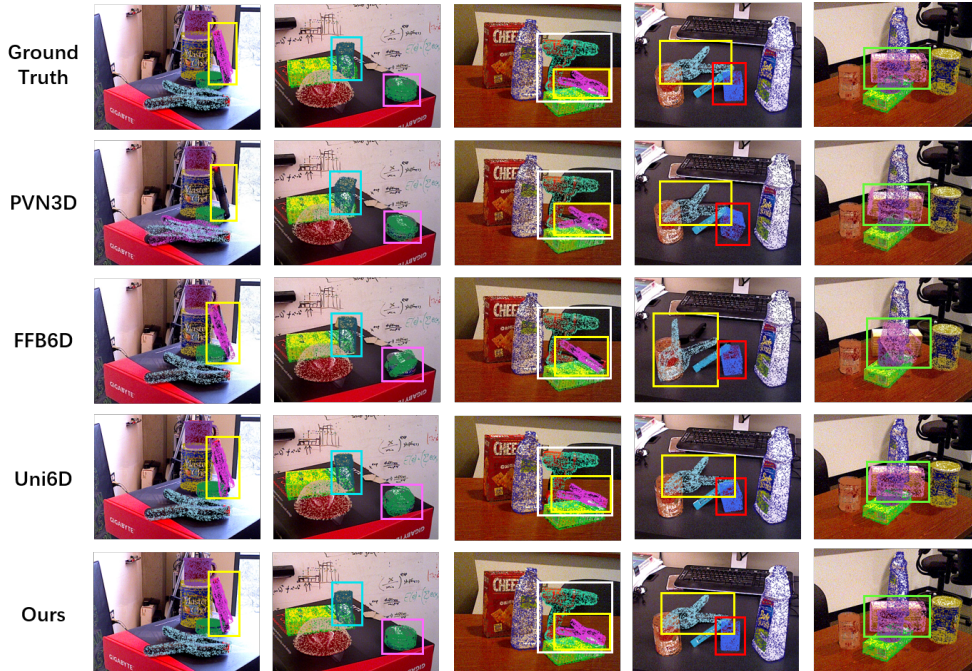


Figure 4: Qualitative results of 6D pose on the YCB-Video dataset.

Table 7: The superiority of reducing real data requirements on the YCB-Video dataset.

real ratio	Uni6D [17]		Denoise with GT		Ours	
	ADD-S	ADD(S)	ADD-S	ADD(S)	ADD-S	ADD(S)
100%	95.04	88.64	97.67	92.52	96.77	91.51
10%	91.84	81.47	97.49	91.36	95.60	88.02
1%	89.95	77.98	97.35	91.29	95.22	86.41
0%	73.52	54.71	97.29	90.52	93.63	84.19

For using synthetic data only, the performance of Uni6D suffers a 21.52% drop, our method only has a performance drop of 3.14%. Meanwhile, the performance of our method using 1% real data is comparable with Uni6D using 100% real data, which proves that our method effectively reduces the need to annotate expensive real data.

4.5 Implementation Details

We adopt ResNet-50 [39] and FPN [40] for Mask R-CNN. The channels of the first convolutional layer are set to 4 for the input RGB-D image. We train the models with 16 NVIDIA GTX 1080Ti GPUs (three images per GPU) for 40 epochs with an SGD optimizer which momentum is 0.9 and weight-decay is 0.0001. The initial learning rate is set to 0.005 with a linear warm-up, and decreased by 0.1 after 15, 25 and 35 epochs. λ_0 in the loss function is set to 1 in epoch [1, 20), 5 in [20, 30), 20 in [30, 38) and 50 in [38, 40], λ_1 and λ_2 are set to 1. Please refer our Appendix for more details.

4.6 Qualitative Results

For intuitively comparing the qualitative results between Uni6Dv2 and other methods [17, 13, 14], we provide some estimation results on the YCB-Video dataset in Fig. 4, with failed results framed by the bounding box. Uni6Dv2 achieves a more precise and robust 6D pose estimation result compared to other state-of-the-art methods when there are few visible points and more noise interference.

5 Conclusion

In this paper, we improve Uni6D from the perspective of denoising. We first investigate the instance-outside and instance-inside noise which have severely limited the original Uni6D’s performance. Then Uni6Dv2 employs a two-step denoising pipeline to address this issue. In the first step, an instance segmentation network is used to filter out instance-outside noise, and in the second step, a lightweight depth denoising module is used to correct instance-inside noise. Extensive experimental results show that our method outperforms other state-of-the-art methods and improves the performance of the original Uni6D with only a slight decrease in inference efficiency.

As limitations, other than noise, the 6D pose estimation method based on the unified network may have other flaws that need to be investigated in order to improve performance further. Furthermore, more elegant denoising methods than cropping and masking from RGB-D data should be investigated. We hope that Uni6Dv2 can be a strong baseline approach to 6D pose estimation and inspires future work.

References

- [1] Alvaro Collet, Manuel Martinez, and Siddhartha S Srinivasa. The moped framework: Object recognition and pose estimation for manipulation. *The international journal of robotics research*, 30(10):1284–1306, 2011.
- [2] Jonathan Tremblay, Thang To, Balakumar Sundaralingam, Yu Xiang, Dieter Fox, and Stan Birchfield. Deep object pose estimation for semantic robotic grasping of household objects. In *Conference on Robot Learning*, pages 306–316, 2018.
- [3] Andreas Geiger, Philip Lenz, and Raquel Urtasun. Are we ready for autonomous driving? the kitti vision benchmark suite. In *2012 IEEE conference on computer vision and pattern recognition*, pages 3354–3361, 2012.
- [4] Danfei Xu, Dragomir Anguelov, and Ashesh Jain. Pointfusion: Deep sensor fusion for 3d bounding box estimation. In *Proceedings of the IEEE conference on computer vision and pattern recognition*, pages 244–253, 2018.
- [5] Xiaozhi Chen, Huimin Ma, Ji Wan, Bo Li, and Tian Xia. Multi-view 3d object detection network for autonomous driving. In *Proceedings of the IEEE conference on Computer Vision and Pattern Recognition*, pages 1907–1915, 2017.
- [6] Eric Marchand, Hideaki Uchiyama, and Fabien Spindler. Pose estimation for augmented reality: a hands-on survey. *IEEE transactions on visualization and computer graphics*, 22(12):2633–2651, 2015.
- [7] Zhengyou Zhang. Microsoft kinect sensor and its effect. *IEEE multimedia*, 19(2):4–10, 2012.
- [8] Tanwi Mallick, Partha Pratim Das, and Arun Kumar Majumdar. Characterizations of noise in kinect depth images: A review. *IEEE Sensors journal*, 14(6):1731–1740, 2014.
- [9] Yinda Zhang and Thomas Funkhouser. Deep depth completion of a single rgb-d image. In *Proceedings of the IEEE Conference on Computer Vision and Pattern Recognition*, pages 175–185, 2018.
- [10] Chris Sweeney, Greg Izatt, and Russ Tedrake. A supervised approach to predicting noise in depth images. In *2019 International Conference on Robotics and Automation (ICRA)*, pages 796–802, 2019.
- [11] Wei Ji, Jingjing Li, Shuang Yu, Miao Zhang, Yongri Piao, Shunyu Yao, Qi Bi, Kai Ma, Yefeng Zheng, Huchuan Lu, et al. Calibrated rgb-d salient object detection. In *Proceedings of the IEEE/CVF Conference on Computer Vision and Pattern Recognition*, pages 9471–9481, 2021.
- [12] Chen Wang, Danfei Xu, Yuke Zhu, Roberto Martín-Martín, Cewu Lu, Li Fei-Fei, and Silvio Savarese. Densefusion: 6d object pose estimation by iterative dense fusion. In *Proceedings of the IEEE/CVF conference on computer vision and pattern recognition*, pages 3343–3352, 2019.

- [13] Yisheng He, Wei Sun, Haibin Huang, Jianran Liu, Haoqiang Fan, and Jian Sun. Pvn3d: A deep point-wise 3d keypoints voting network for 6dof pose estimation. In *Proceedings of the IEEE/CVF conference on computer vision and pattern recognition*, pages 11632–11641, 2020.
- [14] Yisheng He, Haibin Huang, Haoqiang Fan, Qifeng Chen, and Jian Sun. Ffb6d: A full flow bidirectional fusion network for 6d pose estimation. In *Proceedings of the IEEE/CVF Conference on Computer Vision and Pattern Recognition*, pages 3003–3013, 2021.
- [15] Charles R Qi, Hao Su, Kaichun Mo, and Leonidas J Guibas. Pointnet: Deep learning on point sets for 3d classification and segmentation. In *Proceedings of the IEEE conference on computer vision and pattern recognition*, pages 652–660, 2017.
- [16] Charles Ruizhongtai Qi, Li Yi, Hao Su, and Leonidas J Guibas. Pointnet++: Deep hierarchical feature learning on point sets in a metric space. *Advances in neural information processing systems*, 30, 2017.
- [17] Xiaoke Jiang, Donghai Li, Hao Chen, Ye Zheng, Rui Zhao, and Liwei Wu. Uni6d: A unified cnn framework without projection breakdown for 6d pose estimation. *IEEE/CVF Conference on Computer Vision and Pattern Recognition (CVPR)*, 2022.
- [18] Kaiming He, Georgia Gkioxari, Piotr Dollár, and Ross Girshick. Mask r-cnn. In *Proceedings of the IEEE international conference on computer vision*, pages 2961–2969, 2017.
- [19] Yu Xiang, Tanner Schmidt, Venkatraman Narayanan, and Dieter Fox. Posecnn: A convolutional neural network for 6d object pose estimation in cluttered scenes. In *Robotics: Science and Systems (RSS)*, 2018.
- [20] Stefan Hinterstoisser, Stefan Holzer, Cedric Cagniart, Slobodan Ilic, Kurt Konolige, Nassir Navab, and Vincent Lepetit. Multimodal templates for real-time detection of texture-less objects in heavily cluttered scenes. In *2011 international conference on computer vision*, pages 858–865, 2011.
- [21] Mahdi Rad and Vincent Lepetit. Bb8: A scalable, accurate, robust to partial occlusion method for predicting the 3d poses of challenging objects without using depth. In *Proceedings of the IEEE international conference on computer vision*, pages 3828–3836, 2017.
- [22] Bugra Tekin, Sudipta N Sinha, and Pascal Fua. Real-time seamless single shot 6d object pose prediction. In *Proceedings of the IEEE conference on computer vision and pattern recognition*, pages 292–301, 2018.
- [23] Yinlin Hu, Joachim Hugonot, Pascal Fua, and Mathieu Salzmann. Segmentation-driven 6d object pose estimation. In *Proceedings of the IEEE/CVF Conference on Computer Vision and Pattern Recognition*, pages 3385–3394, 2019.
- [24] Alex Kendall, Matthew Grimes, and Roberto Cipolla. Posenet: A convolutional network for real-time 6-dof camera relocalization. In *Proceedings of the IEEE international conference on computer vision*, pages 2938–2946, 2015.
- [25] Alejandro Newell, Kaiyu Yang, and Jia Deng. Stacked hourglass networks for human pose estimation. In *European conference on computer vision*, pages 483–499, 2016.
- [26] Markus Oberweger, Mahdi Rad, and Vincent Lepetit. Making deep heatmaps robust to partial occlusions for 3d object pose estimation. In *Proceedings of the European Conference on Computer Vision (ECCV)*, pages 119–134, 2018.
- [27] Sida Peng, Yuan Liu, Qixing Huang, Xiaowei Zhou, and Hujun Bao. Pvnnet: Pixel-wise voting network for 6dof pose estimation. In *Proceedings of the IEEE/CVF Conference on Computer Vision and Pattern Recognition*, pages 4561–4570, 2019.
- [28] Ross Girshick. Fast r-cnn. In *Proceedings of the IEEE international conference on computer vision*, pages 1440–1448, 2015.
- [29] Gideon Billings and Matthew Johnson-Roberson. Silhonet: An rgb method for 6d object pose estimation. *IEEE Robotics and Automation Letters*, 4(4):3727–3734, 2019.

- [30] Chi Li, Jin Bai, and Gregory D Hager. A unified framework for multi-view multi-class object pose estimation. In *Proceedings of the european conference on computer vision (ECCV)*, pages 254–269, 2018.
- [31] Gu Wang, Fabian Manhardt, Federico Tombari, and Xiangyang Ji. Gdr-net: Geometry-guided direct regression network for monocular 6d object pose estimation. In *Proceedings of the IEEE/CVF Conference on Computer Vision and Pattern Recognition*, pages 16611–16621, 2021.
- [32] Ningkai Mo, Wanshui Gan, Naoto Yokoya, and Shifeng Chen. Es6d: A computation efficient and symmetry-aware 6d pose regression framework. *arXiv preprint arXiv:2204.01080*, 2022.
- [33] Gu Wang, Fabian Manhardt, Jianzhun Shao, Xiangyang Ji, Nassir Navab, and Federico Tombari. Self6d: Self-supervised monocular 6d object pose estimation. In *European Conference on Computer Vision*, pages 108–125, 2020.
- [34] Jason Ku, Ali Harakeh, and Steven L Waslander. In defense of classical image processing: Fast depth completion on the cpu. In *2018 15th Conference on Computer and Robot Vision (CRV)*, pages 16–22, 2018.
- [35] Berk Calli, Arjun Singh, Aaron Walsman, Siddhartha Srinivasa, Pieter Abbeel, and Aaron M Dollar. The ycb object and model set: Towards common benchmarks for manipulation research. In *2015 international conference on advanced robotics (ICAR)*, pages 510–517, 2015.
- [36] Sida Peng, Yuan Liu, Qixing Huang, Xiaowei Zhou, and Hujun Bao. Pvnet: Pixel-wise voting network for 6dof pose estimation. In *Proceedings of the IEEE/CVF Conference on Computer Vision and Pattern Recognition*, pages 4561–4570, 2019.
- [37] Eric Brachmann, Alexander Krull, Frank Michel, Stefan Gumhold, Jamie Shotton, and Carsten Rother. Learning 6d object pose estimation using 3d object coordinates. In *European conference on computer vision*, pages 536–551, 2014.
- [38] Stefan Hinterstoisser, Vincent Lepetit, Slobodan Ilic, Stefan Holzer, Gary Bradski, Kurt Konolige, and Nassir Navab. Model based training, detection and pose estimation of texture-less 3d objects in heavily cluttered scenes. In *Asian conference on computer vision*, pages 548–562, 2012.
- [39] Kaiming He, Xiangyu Zhang, Shaoqing Ren, and Jian Sun. Deep residual learning for image recognition. In *Proceedings of the IEEE conference on computer vision and pattern recognition*, pages 770–778, 2016.
- [40] Tsung-Yi Lin, Piotr Dollár, Ross Girshick, Kaiming He, Bharath Hariharan, and Serge Belongie. Feature pyramid networks for object detection. In *Proceedings of the IEEE conference on computer vision and pattern recognition*, pages 2117–2125, 2017.